The Formation of Subtropical Phytoplankton Blooms Is Dictated by Water Column Stability During Winter and Spring in the Oligotrophic Northwestern North Pacific

K. Matsumoto, Y. Sasai, K. Sasaoka, E. Siswanto, and M. C. Honda

Research Institute for Global Change, Japan Agency for Marine-Earth Science and Technology (JAMSTEC), Yokosuka, Japan.

Correspondence to:

K. Matsumoto,

matsumotok@jamstec.go.jp

Key Points:

- Episodic blooms occurred in warmer water in winter and in cooler water in late spring.
- The blooms were mesoscale or submesoscale and were governed by water column stability.
- The behavior of wintertime mixed-layer depth dictates the magnitude of blooms and the timing of bloom onset and demise.

Abstract Subtropical phytoplankton blooms were observed in winter and late spring (rather than in early spring, as is typical) via shipboard observations in an area south of the Kuroshio Extension in the northwestern North Pacific subtropical gyre. Satellite-based observations revealed that these submesoscale blooms occurred in warmer water masses in winter and in cooler water masses in late spring. The fact that winter blooms occurred in warmer areas suggests that they depend on water column stratification caused by solar heating. In contrast, the fact that the late-spring blooms occurred in cooler areas suggests a breakdown of stratification due to a recurrence of convective mixing. Mesoscale blooms occurred at intermediate water temperatures in early spring, suggesting a repeating sequence of stratification and mixing during this period. Wintertime deep convective mixing in the northwestern North Pacific subtropical gyre creates Subtropical Mode Water. The behavior of the wintertime mixed-layer depth, which determines the thickness of Subtropical Mode Water, also dictates the characteristics of subtropical blooms such as their magnitude and the timing of onset and demise. Based on in situ observations and a model analysis, we conclude that deeper winter mixing, which increases nutrient concentrations, will intensify early-spring blooms and facilitate the formation of episodic blooms in winter and late spring. On the other hand, shallower winter mixing should increase stratification and thus facilitate the formation of smaller blooms, even in winter.

Plain Language Summary In the subtropical northwestern North Pacific, nutrients brought into shallow water by winter mixing were observed to fuel local increases in phytoplankton from winter to late spring. Surprisingly, these increases in phytoplankton occurred in warm waters in winter and in cold waters in late spring. Large increases in phytoplankton require ample supplies of both light and nutrients. Our data suggests that phytoplankton increased in winter in waters that were warmed by solar heating after the cessation of vertical mixing and in late spring in waters that were cooled by the recurrence of vertical mixing. Wintertime mixed-layer depth fluctuates from year to year. Based on field observations and a model analysis, we suggest that the timing and magnitude of phytoplankton increases vary with the depth of the wintertime mixed layer, which in turn affects year-to-year variability of carbon export in this region.

1 Introduction

The North Pacific subtropical gyre (NPSG) has often been referred to as an “ocean desert” because of its low chlorophyll *a* (chl-*a*) concentration, which is caused by its stable water

column structure and nutrient limitation in the euphotic zone. Most biogeochemical studies of this region have been conducted in the central North Pacific as part of the U.S. Joint Global Ocean Flux Study that began in the late 1980s (Karl & Lukas, 1996). In the central NPSG, surface chl-*a* concentrations are low throughout the year, averaging less than 0.1 mg m^{-3}, but vary seasonally with a peak in winter and ebb in summer (Chavez et al., 2011). Interestingly, however, phytoplankton blooms (hereinafter referred to as "blooms") do occur in summer in this region. The processes underlying these blooms include nitrogen fixation, eddy interactions, internal waves, and mixing at the subtropical front (Chow et al., 2017, 2019). Outside of the central North Pacific, the K2S1 project was established in the northwestern North Pacific to compare the biogeochemistry of subarctic and subtropical waters during 2010 and 2011 (Honda et al., 2017). This project involved the creation of a subtropical station in the south of the Kuroshio Extension in the northwestern NPSG (S1: 145°E, 30°N). To understand the underlying mechanisms and causes of the seasonality of biogeochemical cycles, intensive shipboard observations were carried out at S1 in each season during the years 2010 and 2011 (Honda et al., 2017).

In the central NPSG, nitrate concentrations in the surface mixed layer are typically less than 0.01 μmol kg^{-1} throughout the year, as winter mixing generally does not extend beyond a depth of 125 m (Karl et al., 2001). In contrast, the northwestern NPSG is the site of deep wintertime convective mixing, which occasionally extends to a depth of about 200–300 m (Suga & Hanawa, 1990). The homogeneous water mass beneath the thermocline (i.e., after stratification) in the North Pacific is known as Subtropical Mode Water (STMW). The STMW is carried away from its area of formation by lateral advection (Bingham, 1992), and often serves as a nutrient pool in the oligotrophic subtropical ocean because deep convective mixing causes STMW to become enriched in nutrients (Sukigara et al., 2011). Although wintertime nitrate concentrations in the surface mixed layer at S1 are about 1 μmol kg^{-1} (Wakita et al., 2016), nitrate is definitely among the principal factors that limit annual phytoplankton growth; surface nitrate remains depleted in this area in all seasons except winter, and the integral of primary production increases significantly as the nitracline shoals (Matsumoto et al., 2016). This situation is rather similar to that in the subtropical North Atlantic where STMW is formed by deep winter mixing. The occurrence of spring blooms has been reported in this region during field studies conducted as part of the U.S. Joint Global Ocean Flux Study since the late 1980s (Michaels & Knap, 1996).

Phytoplankton blooms, which are major events during the spring in the world's temperate, eutrophic oceans, are generally considered to be caused by an increase of irradiance in a nutrient-replete water column when the surface mixed layer becomes shallower than the critical depth in the spring according to Sverdrup's (1953) classical critical depth hypothesis. Although a variety of mechanisms that differ with respect to the details of the onset process were later proposed to explain the spring phytoplankton bloom (Behrenfeld et al., 2013; Chiswell, 2011; Taylor & Ferrari, 2011; Zarubin et al., 2017), there is no doubt that deepening of the winter mixed layer keeps the concentration of the phytoplankton population low, and spring stratification allows the phytoplankton to accumulate in the surface layer. If a bloom is defined as a large accumulation of phytoplankton near the surface (which can be more easily detected by satellites and can reach higher rates of primary production by taking advantage of the stronger surface irradiance) rather than an increase of phytoplankton biomass throughout the water column, the stratification that follows vertical mixing can trigger a spring bloom. As mentioned above, summer blooms have been reported in the central NPSG, but it has been reported that spring blooms usually do not occur there because winter mixing does not penetrate into the nutricline (Dore et al., 2008). However, even in the oligotrophic subtropical waters of the North Atlantic, spring blooms have often been reported because convective mixing in the winter is deep enough to penetrate the thermocline (Steinberg et al., 2001; Zarubin et al., 2017). At S1, the peak in the seasonal cycle of chl-*a* concentrations is thought to occur in March and April, as inferred from a 16-year timeseries of ocean-color observations (Siswanto et al., 2015). The implication is that a bloom typically occurs in early spring in the northwestern NPSG.

In contrast to the ocean-color observations, however, shipboard observations at S1 have shown a dramatic subtropical bloom during February (Fujiki et al., 2016; Matsumoto et al., 2016). Matsumoto et al. (2016) reported that primary production was highest in February, when it was more than twice the annual average, despite the fact that the depth of winter mixing exceeded the critical depth at the latitude of S1 (Siswanto et al., 2015). Shipboard observations also revealed a bloom at the end of April in the same year that we will discuss later, although nitrate was already depleted within the surface mixed layer at the time (Matsumoto et al., 2016). These observations seem inconsistent with the mechanisms proposed to explain the onset of the spring bloom.

Shiozaki et al. (2014) demonstrated that factors determining spring bloom onset varied with critical depth (Sverdrup, 1953) or the weakening of turbulence (Taylor & Ferrari, 2011) among

subregions such as the Oyashio and Kuroshio region, the STMW region, and its transition region in the northwestern North Pacific. However, they point out that these factors cannot necessarily explain the timing of bloom onset in the STMW region. In this region, the process of bloom formation is thought to be more complex, as it is observed in winter and late spring. The settling of particles at S1 increases significantly from winter to spring (Honda, 2020). It is clear that the formation of blooms during winter and spring has an impact on carbon fluxes. What factors determine the timing of bloom onset, and how does the magnitude of blooms change? Our primary goal in conducting this study was to answer these questions, and thereby to enhance our knowledge of carbon export in the northwestern NPSG.

2 Materials and Methods

2.1 Shipboard sampling and data acquisition

Shipboard observations were conducted from winter to spring at S1 (145°E, 30°N) during 2010 and 2011 as part of the K2S1 Project (Honda et al., 2017). The schedule of each shipboard observation conducted at S1 was as follows: MR10-01, 30 January 2010–10 February 2010; MR11-02, 13 February 2011–18 February 2011; MR11-03, 28 April 2011–30 April 2011. The study site is situated in the northwestern NPSG, south of the Kuroshio Extension (Figure 1a), at a place where the convective mixing that develops in winter is part of the process of STMW formation. The latitude of S1 is near the boundary where the vertical extent of the STMW increases northward and decreases sharply southward to 28°N (Suga & Hanawa, 1990) (Figure 1b). All of our observations are based on water samples that were collected with Niskin-X bottles suspended from a conductivity–temperature–depth (CTD) profiler system, except for surface samples, which were collected with a plastic bucket. The CTD casts were carried out several times during each cruise within a 50-km radius of S1. Nutrient analyses were performed on board using a continuous segmented flow analyzer (QuAAtro 2-HR, BL TEC K.K., Tokyo, Japan) with a detection limit of 0.03 μmol kg^{-1} for nitrate (Wakita et al., 2016). Chl-*a* concentrations were measured using a fluorometer (model 10-AU, Turner Designs, Inc., San Jose, USA) with the conventional acidification method of Holm-Hansen et al. (1965). Particles in 0.5-L water samples were filtered onto a GF/F filter, and chl-*a* was immediately extracted in N,N-dimethylformamide in darkness at −20 °C for 24 h (Suzuki & Ishimaru 1990).

Two types of mixed layer depths (MLDs) were calculated by applying the criterion that the density was either 0.03 kg m^{-3} or 0.125 kg m^{-3} greater than the density at the shallowest depth that could be effectively sampled with the CTD profiler (de Boyer Montégut et al., 2004). The typical MLD calculated with a 0.125 kg m^{-3} criterion gives the top of the seasonal pycnocline, but the depth of the actively turbulent layer is given by a smaller density criterion (Franks, 2015). Chiswell (2011) used a 0.025 kg m^{-3} criterion to represent the depth of the actively turbulent layer, but we chose a 0.03 kg m^{-3} density difference as a practical criterion because a smaller density step was too sensitive to noise. The estimated horizontal distribution of the climatological MLDs around S1 and the seasonal variations of MLDs at the site were obtained from the MIxed Layer dataset of Argo, Grid Point Value (MILA GPV). The MILA GPV dataset was incorporated into a 2° × 2° grid by using quality-controlled Argo 10-d profiles. Values were calculated by using the median at each grid cell, but averaged if the number of datapoints within the grid cell was less than four (Hosoda et al., 2010). In this study, we used data within a 2° × 2° grid centered at S1 that was gridded from averaged values from 2001 to 2010 for the climatological MLDs, though each year's data were averaged from 4° × 4° gridded data. The MLDs were represented by using the 10-d data and monthly averages.

2.2 Satellite-based observations

Daily and monthly composites of chl-*a* concentrations, photosynthetically available radiation (PAR), and sea surface temperature (SST) data were retrieved from Moderate Resolution Imaging Spectroradiometer-Aqua (MODIS) satellite during 2002–2016 as spatial means within a box of dimensions 100 km × 100 km centered at S1. The spatial resolution of the data was 9 km for PAR and SST, but 4 km for chl-*a*. For the years 2002, 2003, 2010, and 2011, the daily composites of chl-*a* for January through May were retrieved separately, but for 2002, the 9-km resolution data from the Sea-viewing Wide Field-of-Sensor (SeaWiFS) were used. The average availabilities of the daily pixel data that could be retrieved from within the 100-km^2 box between January and May were 21% in 2010 (the lowest year) and 32% in 2011 (the highest year). Therefore, in addition to spatial means, the maxima within the box were used to detect patchy blooms. Furthermore, daily composites of chl-*a* concentrations and SSTs with a higher 1-km spatial resolution were acquired more widely within a 2° × 2° grid centered at S1 so that submesoscale (~10 km) and mesoscale (~100 km) phenomena could be detected when skies were

clear in 2010 and 2011. The patchy distributions of subtropical blooms could be detected from the 1-km spatial resolution images. The climatology of monthly critical depths at S1 were estimated from the satellite-based observations (Siswanto et al., 2015). The critical depth is defined as the depth at which bulk phytoplankton growth rate balances the bulk loss rate (Sverdrup, 1953). Briefly, the critical depth was expressed by using the following simplified equation (Parsons et al., 1984):

$$CD = 0.5 \cdot PAR / K_d PAR \cdot I_c$$

where K_dPAR (m^{-1}) is the attenuation coefficient of PAR and I_c (mol quanta m^{-2} d^{-1}) is PAR at the compensation depth. K_dPAR was calculated from K_d490 data which is the attenuation coefficient at 490 nm (Morel et al., 2007). In this study, we used a constant I_c of 1.14 (Shiozaki et al., 2014). The weighting factor of 0.5 was used to reduce PAR due to absorption in water (Parsons et al., 1984).

2.3 Applied model to evaluate the vertical profile of nitrate and phytoplankton biomass

The daily mean output (during 2002–2003) from a coupled three-dimensional, physical-biological model of the North Pacific was used to analyze vertical profiles of nitrate and phytoplankton biomass in the upper 300 m of the water column between January and May at S1. The model produced realistic topographies of simulated mesoscale and submesoscale oceanic structures. We used the Ocean general circulation model For the Earth Simulator (OFES) including sea ice (Komori et al., 2005; Masumoto et al., 2004) coupled to a simple nitrogen-based, four-component (nitrate–phytoplankton–zooplankton–detritus [NPZD]) pelagic model (Oschlies, 2001). The OFES domain extended from 20°S in the South Pacific to 66°N in the North Pacific and from 100°E to 70°W. The horizontal resolution was 1/30° (approximately 3 km), and there were 100 vertical levels that ranged in thickness from 5 m at the surface to 260 m at a maximum depth of 6000 m. The 1/30° OFES simulation is capable of partially resolving submesoscale phenomena, especially at mid- to low latitudes (Qiu et al., 2014; Sasaki et al., 2014). Atmospheric forcing of the simulation was taken from a six-hourly Japanese 25-year reanalysis with 1° resolution (Onogi et al., 2007). The evolution of biological tracers in the OFES was governed by advection–diffusion equations with source and sink terms (ecosystem dynamics). Details of the biological model are described elsewhere (Sasai et al., 2006; Sasai et al., 2010).

The simulation was performed for 2002–2003 to understand how the processes of bloom formation (in terms of timing, demise, and magnitude) respond to the intensity of winter mixing. Our simulation period featured the highest variability of wintertime MLDs in the past 20 years, and the trend was similar to the trend during the period of shipboard observations in 2010 and 2011 (see section 4.2 in the discussion). In addition, we evaluated whether the simulation results were consistent with our interpretation of shipboard observations; namely, our understanding of the impact of oceanic conditions on subtropical blooms.

3 Results

3.1 Seasonal variations of insolation, SST, and concentrations of nitrate and chl-*a* at the surface

Insolation was highest in July and lowest in December. During these months, the monthly average PAR at S1 was >50 and <20 mol quanta m^{-2} d^{-1}, respectively (Figure 2a). It reached 27 mol quanta m^{-2} d^{-1} in February and increased further to nearly 40 mol quanta m^{-2} d^{-1} in April. The monthly average SST was highest at 28 °C in August, but it remained <20 °C between February and April (Figure 2b). We designated the seasons in the northwestern NPSG as follows: winter, December to February; spring, March to May; summer, June to August; and autumn, September to November. The time just before the SST started to increase was equated to the beginning of spring. Although the seasonal difference in SST is only 3–4 °C in the central NPSG (Brix et al., 2004), the temperature difference was nearly 10 °C between winter and summer at S1. Nutrient concentrations were generally low throughout the year. Nitrate concentrations were relatively high with nearly 1 μmol kg^{-1} at the surface during January and February, but were less than 0.2 μmol kg^{-1} after April (Figure 2c). A typical spring bloom was detected by ocean-color observations between the middle of March and the beginning of April (Figure 2d). The annual mean chl-*a* in this region was 0.16 mg m^{-3} (standard deviation: 0.09 mg m^{-3}) at the surface. In this study, a subtropical bloom was defined as an area with a chl-*a* concentration greater than 0.4 mg m^{-3} at the surface, which is more than 2 standard deviations above the annual mean. Shipboard observations revealed subtropical blooms in the beginning of February in 2010 and 2011 and at the end of April in 2011 (Figure. 2d'). These subtropical blooms were remarkable in 2011, and the overall chl-*a* concentrations during winter and spring were higher in 2011 than in 2010 (Figure 2d'). The shipboard observations revealed a massive

winter bloom (0.82 mg m^{-3}) and a moderate late-spring bloom (0.49 mg m^{-3}) in 2011, but these blooms were not apparent when ocean-color observations were averaged spatially within the 100-km^2 box around S1 (Figure 2d'). However, we were able to identify blooms within the box from ocean-color observations in 2011 through the analysis of maxima; these maxima reached chl-*a* concentrations comparable to shipboard observations. The winter bloom of 2010 could not be identified through the analysis of maxima (Figure 2d'). With less than 32% of valid pixels in the 100-km^2 box, it was difficult to reliably capture bloom formation when data were averaged spatially. This issue of spatial resolution and valid pixels may well be the cause of the discrepancy between in situ chl-*a* concentrations and ocean-color estimates (Figure 2d'). This indicates that subtropical blooms in this region form rather patchy submesoscale blooms.

When surveying a wider area around S1 with a higher 1-km spatial resolution in 2010 and 2011, mesoscale and submesoscale blooms were clearly detectable in ocean-color images in both winter and spring (Figure 3). However, we were only able to clearly capture the blooms on the dates shown in this figure, and the images were not available during the shipboard observation periods as there were few clear days without clouds. The images acquired during winter showed higher concentrations of chl-*a* within blooms in 2011. Images of spring blooms were acquired during an earlier period in 2010 and during a later period in 2011. The horizontal extent of blooms were patchy in both periods, but more extensive in spring. The higher resolution satellite data were capable of capturing the occurrences of mesoscale and submesoscale blooms in detail around the study area. Interestingly, these data show that a winter bloom can occur in water that is slightly warmer than the surrounding water, whereas an early-spring bloom can occur in water that is slightly cooler than the surrounding water, and a late-spring bloom can occur in water that is even cooler still relative to the surrounding water. These relationships were revealed by the chl-*a* concentration and SST data (Figure 3). The peaks of the chl-*a* concentrations during the winter appeared in water masses with temperatures of 19.0–19.5 °C and 18.5–19.0 °C in 2010 and 2011, respectively (see arrows in Figure 3). Similar chl-*a* peaks in early and late spring appeared in water masses with temperatures of ~18.5 °C in 2010 and 17.5–18.0 °C in 2011 (see arrows in Figure 3). Although the increasing insolation from February to April would logically be expected to cause SSTs to increase (Figure 2a), the above results indicate that the winter bloom occurred in a warmer water mass than the late-spring bloom.

3.2 Mixed layer depth and light availability

Seasonal variations of MLDs and critical depths at S1 were examined from January to May in 2010 and 2011 to elucidate the factors that control subtropical blooms (Figure 4; upper panels). The MLDs were defined based on density differences of either 0.03 kg m^{-3} ($MLD_{0.03\sigma\theta}$) or 0.125 kg m^{-3} ($MLD_{0.125\sigma\theta}$), and were calculated from 10-d MILA GPV data and superimposed in-situ data from shipboard observations. MLDs estimated from MILA GPV data and in-situ data were quite similar. The depth of active turbulence roughly corresponds to $MLD_{0.03\sigma\theta}$ and can be considered to be the concurrent depth of mixing. The top of the seasonal pycnocline is given by $MLD_{0.125\sigma\theta}$ and can be considered to be a metric of the strongest mixing during the recent past. We think it is reasonable to use the $MLD_{0.03\sigma\theta}$ to capture the onset of stratification and the $MLD_{0.125\sigma\theta}$ to estimate the depth of convective mixing. In 2010, the $MLD_{0.125\sigma\theta}$ deepened episodically to nearly 200 m in early February, but in other periods, it remained shallower than 150 m. In 2011, the $MLD_{0.125\sigma\theta}$ largely remained deeper than 150 m until early April, and the $MLD_{0.125\sigma\theta}$ episodically deepened to 320 m and the $MLD_{0.03\sigma\theta}$ to around 200 m in late March. The $MLD_{0.03\sigma\theta}$ did not differ much between 2010 and 2011, except in late March 2011. The $MLD_{0.125\sigma\theta}$ was shallower than 60 m after mid-April in both years, indicating that seasonal stratification intensified from around this time. Winter convective mixing was shallow in 2010 and deep in 2011, as seen from the $MLD_{0.125\sigma\theta}$. This indicates that winter mixing was easier to develop in 2011. However, the $MLD_{0.03\sigma\theta}$ indicates that the stratification depths in both years were similar. This implies that mixing developed more frequently, but not continuously, in 2011.

Monthly averages of critical depth tended to deepen as insolation increased. According to the classical understanding of spring blooms (Sverdrup, 1953), it is necessary that the MLD be shallower than the critical depth before a bloom can be initiated. Phytoplankton growth was undoubtedly restricted by light limitation during January, because both $MLD_{0.125\sigma\theta}$ and $MLD_{0.03\sigma\theta}$ were deeper than the critical depth in most cases. This implies that the upper water column was turbulent to the vicinity of the critical depth on a regular basis. In February, the $MLD_{0.125\sigma\theta}$ was still deeper than the critical depth in many cases, but the $MLD_{0.03\sigma\theta}$ was much shallower than the critical depth in some cases. The implication is that light availability was much improved by episodic stratification after February. In March, when winter mixing developed as in 2011, the relationship between MLD and critical depth was similar to that in February, but in 2010, when winter mixing was weak, both MLDs were much shallower than the

critical depth. Light limitation may have occurred during February and March, when convective mixing was most developed, but light would no longer have been limiting after April because both MLDs were much shallower than the critical depth.

3.3 Typical vertical profiles of nitrate and chl-*a* concentrations as a function of water column stability

Five typical vertical profiles of in situ nitrate and chl-*a* concentrations based on water column stability were extracted from shipboard observations (Figure 4; lower panels). Types A and B are from winter 2010, C is from winter 2011, and D and E are from spring 2011. The depth ranges with homogeneous temperature, nitrate, and chl-*a* in these vertical profiles roughly confirm that the depth of the actively turbulent layer is given by the $MLD_{0.03\sigma\theta}$, and the top of the seasonal pycnocline is given by the $MLD_{0.125\sigma\theta}$.

Type A: Winter convective mixing had not yet developed. This profile was observed at the end of January in 2010, and both the $MLD_{0.03\sigma\theta}$ and $MLD_{0.125\sigma\theta}$ were still as shallow as 61 m and 87 m, respectively. An influx of nutrients sufficient to fuel a bloom in the mixed layer could not occur in the absence of winter mixing. The high temperature of the surface mixed layer indicated that it had not yet been stirred deeply. A slight increase of chl-*a* was observed at the bottom of the $MLD_{0.03\sigma\theta}$, but the low concentration of nitrate (<0.1 μmol kg^{-1}) in the $MLD_{0.03\sigma\theta}$ precluded the formation of a bloom.

Type B: Winter convective mixing began to develop. This profile was observed in early February of 2010, during which both the $MLD_{0.03\sigma\theta}$ and the $MLD_{0.125\sigma\theta}$ were deepened to 173 m and 183 m, respectively. Both MLDs were deeper than the critical depth, which supplied high concentrations of nitrate into the surface mixed layer. Thorough mixing of the water column resulted in uniform water properties as the temperature decreased. Nitrate concentrations were as high as 0.7 μmol kg^{-1}, but chl-*a* was as low as 0.3 mg m^{-3} within the $MLD_{0.03\sigma\theta}$.

Type C: The water column stratified after a period of winter mixing. This profile was observed in the middle of February 2011, at which time the $MLD_{0.03\sigma\theta}$ was as shallow as 66 m, though the $MLD_{0.125\sigma\theta}$ was still as deep as 209 m. The low SST suggests that this profile occurred immediately after the onset of stratification. There was a very distinct subtropical bloom associated with chl-*a* concentrations exceeding 0.8 mg m^{-3} at the surface, since both light and

nutrients were available within the shallow $MLD_{0.03\sigma\theta}$. The chl-*a* could have been even higher after this because there was a residual nitrate concentration that exceeded 0.4 μmol kg^{-1} within the $MLD_{0.03\sigma\theta}$.

Type D: Stratification intensified as the season progressed. This profile was observed at the end of April in 2011, at which time the $MLD_{0.03\sigma\theta}$ and the $MLD_{0.125\sigma\theta}$ had shoaled to 16 m and 40 m, respectively. The surface chl-*a* concentration was as low as 0.2 mg m^{-3} due to nitrate depletion in the layer shallower than $MLD_{0.125\sigma\theta}$. But the chl-*a* concentration increased abruptly to 0.9 mg m^{-3} at the subsurface chl-*a* maximum, since light should have been able to penetrate below the $MLD_{0.125\sigma\theta}$ because of the low chl-*a* concentrations in the surface mixed layer.

Type E: Stratification had broken down. This profile was observed at the end of April in 2011, at which time the $MLD_{0.125\sigma\theta}$ had deepened to 71 m, although the $MLD_{0.03\sigma\theta}$ had already shoaled to 33 m. The seasonal pycnocline should be shallow toward spring, but convective mixing developed again. The fact that the SST was relatively low for the time of year, compared to the type D profile, indicates that the water column was well mixed to the $MLD_{0.125\sigma\theta}$. Nutrients should have been progressively consumed during the seasonal enhancement of stratification, but an influx of nutrients occurred when the stratification was disrupted and the water column mixed. Because the critical depth was quite deep at this time of year, there was no light limitation. Nitrate concentrations were already low within the $MLD_{0.03\sigma\theta}$, but chl-*a* concentrations were distributed uniformly within the $MLD_{0.125\sigma\theta}$ from the surface, where the concentrations exceeded 0.5 mg m^{-3}. The implication is that the resupplied nutrients from the breakdown of stratification caused a subtropical bloom in late spring.

4 Discussion

4.1 Factors dictating the formation of subtropical blooms

Our study region south of the Kuroshio Extension is situated in the northwestern NPSG, and both ocean-color and shipboard observations revealed subtropical blooms there during winter and spring. When the observation domain was regarded as the spatial distribution of a 100-km^2 box, patchy blooms that corresponded to chl-*a* maxima were observed, especially in mid-winter and late spring. However, these blooms could not be detected in satellite data with areal smoothing (Figure 2d'). It is possible that our shipboard observations were also able to capture these patchy

blooms. Our results imply that the winter and late-spring blooms are rather sporadic submesoscale phenomena. In contrast, blooms that occurred from late March to early April could be detected with ocean-color data even with areal smoothing (Figure 2d). This indicates that blooms are more widespread, mesoscale phenomena at this time of year. Figure 5 is a conceptual illustration of subtropical bloom formation in winter, early spring, and late spring as a function of water column stability based on the climatological MLDs and critical depth. Although every bloom is triggered by an increase in the availability of both light and nutrients, our findings indicate that the onset, demise, and magnitude of these subtropical blooms are governed by water column stability, which varies throughout the year.

4.1.1 Winter bloom

In winter, classical theory indicates that light becomes a limiting factor for phytoplankton growth in the northwestern NPSG because winter convective mixing occasionally extends to a depth of about 200–300 m during the formation of STMW (Suga & Hanawa, 1990). Winter mixing creates high nutrient concentrations in the surface mixed layer as in the Type B profile (Figure 4), and subsequent stratification triggers a winter bloom as in the Type C profile (Figure 4). Such phenomena have previously been described as “stratification-onset” (Chiswell, 2011) and “convection-shutdown” (Ferrari et al., 2015; Taylor & Ferrari, 2011) mechanisms. These mechanisms are not inconsistent with basic critical depth theory, but they imply that a decrease of active turbulence (i.e., stratification) is an important factor that leads to shoaling of the mixed layer. In addition, Zarubin et al. (2017) recently proposed a “Dispersion-Confinement” mechanism to account for subtropical blooms. They suggested that phytoplankton can increase rapidly in response to stratification because phytoplankton can maintain a high growth rate even during the deep convective mixing in winter, although the phytoplankton population is dispersed and diluted. The effects of light limitation may be small in winter if this mechanism can be applied to this region, and the high growth rate of phytoplankton may allow subtropical blooms to form rapidly, even if stratification is episodic.

Our shipboard and ocean-color observations indicate the occurrence of submesoscale blooms in winter. A winter bloom should develop when there is a weakening of atmospheric forcing due to factors such as cooling and wind-driven mixing. This weakening can enhance stratification. It is unclear whether such reductions of atmospheric forcing occur episodically in a limited area in

mid-winter, when the mixed layer usually develops. However, the eddy-driven stratification proposed by Mahadevan et al. (2012) may be an example of a kind of forcing that suppresses convective mixing. Their conceptualization of the stratification process is based on forcing during which relatively dense water slides laterally beneath water that is less dense in a region where there is a horizontal density gradient. They have indicated that this forcing leads to a patchy, submesoscale bloom in winter that advances the time of the normal spring bloom by 20–30 d in high-latitude regions. At the longitude of S1, deep convective mixing homogenizes the water vertically, and although cooling in the area north of 30°N leads to formation of STMW, surface stratification develops further south because of solar heating (Suga & Hanawa, 1990). It can therefore be expected that a horizontal density gradient with denser (colder) water in the north and less dense (warmer) water to the south would lead to the creation of vertical stratification during the winter at S1.

The winter bloom resulted in primary production as high as 71 mmol C m^{-2} d^{-1} throughout the water column at S1 (Matsumoto et al., 2016), with surface-water primary production reaching 2.5 mmol C m^{-3} d^{-1} (data not shown). However, the concentration of nitrate introduced into the surface mixed layer by convective mixing was less than 1 μmol kg^{-1} even when mixing was fully developed as in the Type B profile (Figure 4). We calculated how long the bloom could persist at this nitrate concentration, assuming that the water column was stable and unstirred. If the C/N ratio in the phytoplankton equaled the Redfield ratio of 6.6 mol mol^{-1}, nitrogen uptake by phytoplankton when primary production occurs as described above was calculated as 0.38 mmol N m^{-3} d^{-1} at the surface. Then, if the *f*-ratio (the fraction of primary production fueled by nitrate) is assumed to be 0.5, phytoplankton should require about 0.2 μmol kg^{-1} of nitrate per day. The implication is that almost all of the nitrate introduced into the surface water via convective mixing would be consumed within a week. The winter bloom occurred in water that was warmer than the surrounding water because of stratification, but the chl-*a* concentration tended to decrease if the SST increased further (Figure 3). Hence, the phytoplankton population decreased if stratification persisted. However, if convective mixing were to recur, the phytoplankton population would be dispersed, and the bloom would come to an end. The implication is that a bloom of phytoplankton occurs in the winter when there is an increase of the availability of nutrients, but such blooms are submesoscale phenomena that come to an end within a short period of time.

4.1.2 Early-spring bloom

The classical theory indicates that seasonal stratification after the development of winter mixing will lead to a bloom in the subtropics. Subtropical blooms were identifiable in 100-km^2 spatial means of daily composites chl-*a* in the northwestern NPSG in the early spring, but not in winter or late spring (Figure 2d). This suggests that the early-spring blooms are either mesoscale or are composed of numerous submesoscale patches. As already mentioned in section 4.1.1, entrained nutrients should be depleted within a week under stratified conditions. The development of winter mixing differed greatly between 2010 and 2011, but in both years the $MLD_{0.03\sigma\theta}$ became shallower compared to the $MLD_{0.125\sigma\theta}$ from March to April (Figure 4). This divergence of the $MLD_{0.03\sigma\theta}$ and $MLD_{0.125\sigma\theta}$ indicates that the water column was unstable, and the sequence of stratification and mixing could have occurred repeatedly within the gap between the MLDs during this time. Although early-spring blooms occurred in waters with cooler SSTs than winter blooms, in contrast to the late-spring bloom, they did not occur in the lowest SST waters in the area at the time (Figure 3). This means that either stratification or mixing was not unilaterally enhanced. Instead, a fluctuating sequence of stratification and mixing within the MLD gap allowed for the use of both light and nutrients. This gap appears to be greatest in March as seen in the monthly averaged climatology (Figure 5). In addition, light was steadily becoming more available when the water column was stratified during March due to the deepening of the critical depth (Figure 5). If phytoplankton maintain a high growth rate during deep winter mixing as suggested by Zarubin et al. (2017), this instability of the water column could facilitate the subtropical blooms observed in early spring.

4.1.3 Late-spring bloom

Stratification generally intensified rapidly in April (Figure 5). This stable water column led to nutrient depletion within the stratified surface water, and phytoplankton tended to form subsurface maxima typical of the Type D profile (Figure 4). However, shipboard observations revealed a submesoscale bloom at the end of April that was confirmed by the analysis of ocean-color maxima in the 100-km^2 box (Figure 2d'). At this time, the presence of a Type E profile indicated that nitrate was resupplied by stratification breakdown (Figure 4). But how did stratification break down in late spring, despite the likelihood that the weakening of atmospheric forcing as the season progressed would enhance stratification?

It is well known that nutrients can be supplied by mesoscale ocean eddies. A cyclonic eddy enhances primary production because of upwelling inside the eddy (Falkowski et al., 1991). For example, uplift of the nutricline within a cyclonic eddy increased subsurface phytoplankton during the stratified autumn season in the northwestern NPSG (Honda et al., 2018). However, an anti-cyclonic eddy seems to be more important, especially in the subtropical ocean during winter because the downwelling associated with passage of an anti-cyclonic eddy is especially likely to deepen convective mixing inside the eddy (Dufois et al., 2016; Kouketsu et al., 2012). Mesoscale eddies frequently pass through this region (Inoue & Kouketsu, 2016; Kouketsu et al., 2016) so that the passage of an anti-cyclonic eddy may break down stratification and thereby provide nutrients in the northwestern NPSG until late spring. Moreover, interactions between anti-cyclonic and cyclonic eddies will also generate submesoscale vertical upwelling that causes subtropical blooms (Chow et al., 2017, 2019). In addition, the extratropical cyclones that pass by the south coast of Japan and are called south-coast cyclones in Japan (Ueda et al., 2017) may pass by in April, although they occur most frequently in winter. Such eddies and cyclones should be considered as major processes that enhance mesoscale and submesoscale nutrient fluxes to the surface layer in late spring in the northwestern NPSG.

The fact that late-spring blooms occurred in water masses with temperatures of 17.5–18.0 °C in 2011, which was lower than the temperatures of 18.5–19.0 °C associated with winter blooms during the same year (compare winter / spring temperatures indicated by arrows in Figure 3), supports the above-mentioned scenario. That is, convective mixing in late spring has reached the depth of STMW because the typical temperature of STMW is 15–20 °C (e.g., Suga et al., 1989). However, this interpretation implicitly assumes that late-spring blooms are sporadic submesoscale events that occur when an oceanic eddy or south-coast cyclone passes by, because surface stratification is more robust in late spring than in early spring. The mechanism responsible for the late-spring bloom would be basically consistent with the mechanism responsible for the phenomenon called the “autumn bloom,” which occurs when nutrients are resupplied through a breakdown of stratification caused by a reactivation of convective mixing in autumn (Findlay et al., 2006).

4.2 Model analysis of bloom formation with the behavior of wintertime MLDs and its implications for biogeochemistry

Shipboard and satellite observations suggest that the formation of mesoscale or submesoscale blooms in the northwestern NPSG during winter and late spring depends on the stability of the water column. In the subtropical Atlantic, which is also a site of STMW formation, it has been suggested that spring blooms become more intense with deeper winter mixing (Michaels & Knap, 1996). Our observations also show that deeper winter mixing tends to enhance subtropical blooms because the chl-*a* concentrations estimated both from the ship and from ocean-color observations were higher in 2011 than in 2010, and blooms were evident in the winter and also in the late spring of 2011 (Figure 2d'). The thickness of STMW reflects the deepening of convective mixing during winter. An anti-cyclonic eddy weakens ocean stratification, deepens the thermocline, and links mixed layer development with STMW formation (Kouketsu et al., 2012; Uehara et al., 2003). Variations of STMW thickness are also associated with the dynamic state of the Kuroshio Extension (Oka et al., 2015) and the activity of the Aleutian Low (Sugimoto & Hanawa, 2010). The thickness of STMW could be expected to influence the formation of subtropical blooms via bottom-up control, because the influx of nutrients is enhanced by more active winter convective mixing.

We examined interannual variations of monthly MLDs from winter to spring over the last 20 years (Figure 6). The MLDs deepened from 2010 to 2011, especially in the February–March period. In the STMW formation area, a previous investigation of the long-term behavior of the wintertime MLD identified considerable decadal variation after the late 1980s and revealed the deepening of wintertime MLDs from the late 1990s to the mid-2000s (Sugimoto & Kako, 2016). We also identified a deepening of winter mixing from 2002 to 2003, and we found that the magnitude of fluctuation in MLDs during this period was the largest in the last 20 years. The development of winter mixing should enhance the availability of nutrients, which can boost phytoplankton growth, while also decreasing light availability, which has the opposite effect.

We carried out a model analysis with a coupled 3-D physical–biological model from 2002 to 2003 to evaluate how the intensity of winter mixing affects bloom formation with a particular focus on the dynamics of nitrate concentrations and phytoplankton biomass during winter and spring at S1 (Figure 7). Our model closely reproduced the MLDs estimated from MILA GPV

during this period, showing that winter mixing was more active in 2003 than in 2002. In 2002, the spatial means of ocean-color-derived chl-*a* in the 100-km^2 box were relatively constant, with low concentrations of around 0.2 mg m^{-3} persisting from January to early April, although the maxima analysis captured frequent spikes of around 0.4 mg m^{-3}. This indicates that weak, submesoscale blooms likely occurred during this period. However, both mean and maximal chl-*a* concentrations decreased to around 0.1 mg m^{-3} after mid-April. In 2003, the concentrations of ocean-color chl-*a* clearly increased from late March to early April, when a massive bloom was observed with chl-*a* of 0.84 mg m^{-3} in the maxima analysis. Blooms were not detected during the rest of 2003, and chl-*a* decreased to about 0.1 mg m^{-3} by mid-April as in 2002. The timings of bloom formation were in good agreement with our simulation results. As discussed below, our simulations produced the typical vertical profiles of nitrate and chl-*a* concentrations derived from water column stability shown in Figure 4, and highlighted how the characteristics of bloom formation are affected by the intensity of winter mixing.

In 2002 (Figure 7; left panel), there was little winter mixing until the middle of January, and phytoplankton biomass remained low because of a lack of nitrate in the shallow $MLD_{0.125\sigma\theta}$ (Type A). Deepening of vertical mixing increased nitrate concentrations, but phytoplankton biomass remained low within the $MLD_{0.125\sigma\theta}$ at the end of January (Type B). Phytoplankton biomass increased in the $MLD_{0.03\sigma\theta}$ because of stratification immediately afterward (Type C), but nitrate was depleted at that depth at the beginning of February. After the middle of April, nitrate was depleted at depths shallower than about 50 m as stratification intensified, and phytoplankton formed a subsurface maximum (Type D). From the middle of February to early April, the MLDs fluctuated with repeated episodes of intensified mixing and stratification, and phytoplankton biomass increased in the $MLD_{0.03\sigma\theta}$. This water column instability and enhancement of phytoplankton biomass is consistent with the MILA GPV and ocean-color data. This appears to have been a repeat of profiles B, C, D, and E, although the ocean-color data indicated that the magnitude (chl-*a* concentration and areal extent) of any subtropical blooms was not large. Because there was less winter mixing that year, the influx of nutrients was low, and blooms did not develop during this period. However, a repetition of the stratification and mixing during this period might have been easier and could have resulted in a persistent bloom.

In 2003 (Figure 7; right panel), there was little winter mixing until the middle of January, as in 2002 (Type A). Subsequently, winter mixing was much better developed than in 2002. High

nitrate concentrations were supplied to the surface mixed layer until the end of March, but the increase of chl-*a* was muted (Type B). Our simulation did indicate that episodic stratification occurred at the beginning of April, although the MILA GPV data showed an earlier initiation of stratification in the middle of March. Such stratification can lead to bloom development as in Type C, and a massive bloom was identified both in the simulation and in ocean-color data. Because nitrate concentrations were still high beneath the stratification depth due to the development of winter mixing, there may also have been a bloom associated with a resupply of nitrate via a breakdown of stratification analogous to Type E. After mid-April, phytoplankton formed a subsurface maximum as the stratification became more robust in a manner that resembles Type D.

The simulation results suggest that the behavior of wintertime MLD, which determines the thickness of STMW, dictates the characteristics of subtropical blooms, including the magnitude of the bloom and the timing of the onset and demise thereof. In years of deep winter mixing, subtropical blooms are expected to be more intense in spring due to elevated nutrient concentrations. However, if episodic stratification occurs, this study suggests that a massive bloom can occur even in winter. When winter mixing develops, high concentrations of nutrients can become stored in the gap between the $MLD_{0.03\sigma\theta}$ and $MLD_{0.125\sigma\theta}$, even if nutrients are consumed fully within the stratified $MLD_{0.03\sigma\theta}$. The episodic breakdown of stratified $MLD_{0.03\sigma\theta}$ is expected to occur easily under this condition, because the water mass within the $MLD_{0.125\sigma\theta}$ is relatively homogeneous. Therefore, in years of deep winter mixing, subtropical blooms are likely to intensify in the form of episodic winter and late-spring blooms in addition to early-spring blooms caused by seasonal stratification. In contrast, during years of weak winter mixing, a low influx of nutrients is likely to weaken any subtropical blooms. Our results suggest that a massive bloom is unlikely to occur in such years, but also indicate that subtropical blooms could form more easily even in winter due to the increased likelihood of stratification.

The behavior of the wintertime MLD may change the quality of the subtropical bloom based on the concentrations of nutrients entrained in the mixed layer. Shipboard observations at S1 have previously revealed that the abundance of large diatoms in winter was low in 2010 but high in 2011 (Fujiki et al., 2016). Phytoplankton communities generally change in structure to relatively large cells in response to an increase of nutrient availability (Irwin et al., 2006). In addition, the net growth of large diatoms may be accelerated by a lower rate of predation in this region,

because the observed primary production in the winter of 2011 was much higher than the carbon demands of mesozooplankton in the surface layer (Kobari et al., 2016). These results suggest that massive blooms tend to be composed of large diatoms in years of deep winter mixing because the nutrient concentrations are high. By contrast, picophytoplankton would be expected to dominate in years of weak winter mixing, even in years when there is a bloom (e.g., the 2002 simulation), because nutrient concentrations during these years are low in the sunlit layer. A subtropical bloom dominated by large diatoms should make a disproportionately large contribution to carbon export in the oligotrophic subtropical ocean, because particulate organic carbon (POC) flux increases monotonically with biogenic opal flux in this region (Honda et al., 2018).

At latitudes near the boundary where the vertical extent of the STMW increases northward and decreases sharply southward, as in the present study area at S1, eddy-driven stratification (Mahadevan et al., 2012) may occur frequently during winter. The export of POC from the surface ocean to depth is likely to be most effective when caused by eddy-driven subduction in conjunction with eddy-driven stratification during a phytoplankton bloom; this mechanism contributes as much as half of the total export of POC in the Kuroshio extension (Omand et al., 2015). Furthermore, submesoscale blooms associated with stratification breakdowns due to eddy interaction or cyclones are expected even in late spring. In addition to the general spring blooms associated with seasonal stratification after winter mixing, episodic blooms contribute to POC formation from winter to late spring. Time-series observations show that settling particles collected at S1 are largest in winter and spring and undergo substantial seasonal and interannual variability (Honda, 2020). Our study suggests that changes in the magnitude of the bloom and the timing of the onset and demise are associated with the behavior of the wintertime MLD and contribute to the seasonal and interannual variability of carbon export.

5 Conclusions

We used comprehensive analysis of shipboard and satellite observations and model simulations to identify the factors that dictate the onset and demise of subtropical blooms in the northwestern NPSG, which differs from the dynamics that operate in the central NPSG. The northwestern NPSG is characterized by the formation of STMW by deep winter mixing and by large interannual variations in wintertime MLD. When a relatively thick STMW layer is formed, high

nutrient concentrations are entrained into the surface mixed layer. This entrainment increases the magnitude of blooms that result from subsequent stratification. Moreover, entrainment enables the recurrence of blooms if stratification subsequently breaks down, even if nutrient concentrations are low in the stratified water. When a relatively thin STMW layer is formed, the concentrations of nutrients entrained in the mixed layer are relatively low, but light availability remains good because the water column is easily stratified. Under these conditions, a subtropical bloom can persist for a long time because the instability of the water column leads to multiple cycles of convective mixing and stratification. Our results indicate that the northwestern NPSG is the site not only of mesoscale blooms caused by seasonal stratification but also of submesoscale blooms associated with episodic stratification and stratification breakdowns. Satellites are now equipped with higher resolution ocean-color sensors, meaning that further detailed observations are likely to improve our understanding of the impact of patchy episodic blooms on carbon export in the northwestern NPSG.

Acknowledgments

We acknowledge the technicians of Marine Works Japan Ltd. for their help with water sampling and onboard analyses. We also thank the crews of the R/V Mirai for their cooperation in the field. We are grateful to our three anonymous reviewers for their constructive comments, which helped improve the manuscript. A part of this work was financially supported by Grants-in-Aid for Scientific Research (KAKENHI JP18H04144) funded by the Ministry of Education, Culture, Sports, Science, and Technology-Japan (MEXT), and a grant (CAF2017-RR02-CMY-Siswanto) from the Asia-Pacific Network for Global Change Research (APN).

Data availability statement

The data discussed in this manuscript are available through the following websites.

Ocean-color data: http://oceancolor.gsfc.nasa.gov

MILA GPV: http://www.jamstec.go.jp/ARGO/argo_web/argo/?lang=en

Cruise data: some data are merged in https://ebcrpa.jamstec.go.jp/k2s1/en/index.html, but more detailed data from specific cruises are available at:

MR10-01 Leg1 (2010-01-19 – 2010-02-06): https://doi.org/10.17596/0001821

MR10-01 Leg2 (2010-02-07 – 2010-02-24): https://doi.org/10.17596/0001822

MR11-02 (2011-02-11 – 2011-03-09): https://doi.org/10.17596/0001830

MR11-03 (2011-04-14 – 2011-05-05): https://doi.org/10.17596/0001831

References

Behrenfeld, M. J., Doney, S. C., Lima, I., Boss, E. S., & Siegel, D. A. (2013). Annual cycles of ecological disturbance and recovery underlying the subarctic Atlantic spring plankton bloom. *Global Biogeochemical Cycles, 27*(2), 526-540. https://doi.org/10.1002/gbc.20050

Bingham, F. M. (1992). Formation and spreading of subtropical mode water in the North Pacific. *Journal of Geophysical Research: Oceans, 97*(C7), 11177-11189. https://doi.org/10.1029/92JC01001

Brix, H., Gruber, N., & Keeling, C. D. (2004). Interannual variability of the upper ocean carbon cycle at station ALOHA near Hawaii. *Global Biogeochemical Cycles, 18*(4). https://doi.org/10.1029/2004gb002245

Chiswell, S. M. (2011). Annual cycles and spring blooms in phytoplankton: don't abandon Sverdrup completely. *Marine Ecology Progress Series, 443*, 39-50. https://doi.org/10.3354/meps09453

Chavez, F. P., Messié, M., & Pennington, J. T. (2011). Marine primary production in relation to climate variability and change. *Annual Review of Marine Science,* 3(1), 227-260. doi:10.1146/annurev.marine.010908.163917

Chow, C. H., Cheah, W., & Tai, J.-H. (2017). A rare and extensive summer bloom enhanced by ocean eddies in the oligotrophic western North Pacific Subtropical Gyre. *Scientific Reports, 7*(1), 6199. https://doi.org/10.1038/s41598-017-06584-3

Chow, C. H., Cheah, W., Tai, J.-H., & Liu, S.-F. (2019). Anomalous wind triggered the largest phytoplankton bloom in the oligotrophic North Pacific Subtropical Gyre. *Scientific Reports, 9*(1), 15550. https://doi.org/10.1038/s41598-019-51989-x

de Boyer Montégut, C., Madec, G., Fischer, A. S., Lazar, A., & Iudicone, D. (2004). Mixed layer depth over the global ocean: An examination of profile data and a profile-based climatology. *Journal of Geophysical Research, 109,* C12003. https://doi.org/10.1029/2004jc002378

Dore, J. E., Letelier, R. M., Church, M. J., Lukas, R., & Karl, D. M. (2008). Summer phytoplankton blooms in the oligotrophic North Pacific Subtropical Gyre: Historical perspective and recent observations. *Progress in Oceanography, 76*(1), 2-38. https://doi.org/10.1016/j.pocean.2007.10.002

Dufois, F., Hardman-Mountford, N. J., Greenwood, J., Richardson, A. J., Feng, M., & Matear, R. J. (2016). Anticyclonic eddies are more productive than cyclonic eddies in subtropical gyres because of winter mixing. *Science Advances, 2*(5), e1600282. https://doi.org/10.1126/sciadv.1600282

Falkowski, P. G., Ziemann, D., Kolber, Z., & Bienfang, P. K. (1991). Role of eddy pumping in enhancing primary production in the ocean. *Nature,* 352(6330), 55-58. doi:10.1038/352055a0

Ferrari, R., Merrifield, S. T., & Taylor, J. R. (2015). Shutdown of convection triggers increase of surface chlorophyll. *Journal of Marine Systems, 147,* 116-122. https://doi.org/10.1016/j.jmarsys.2014.02.009

Findlay, H. S., Yool, A., Nodale, M., & Pitchford, J. W. (2006). Modelling of autumn plankton bloom dynamics. *Journal of Plankton Research, 28*(2), 209-220. https://doi.org/10.1093/plankt/fbi114

Franks, P. J. S. (2015). Has Sverdrup's critical depth hypothesis been tested? Mixed layers vs. turbulent layers. *ICES Journal of Marine Science, 72*(6), 1897-1907. https://doi.org/10.1093/icesjms/fsu175

Fujiki, T., Sasaoka, K., Matsumoto, K., Wakita, M., & Mino, Y. (2016). Seasonal variability of phytoplankton community structure in the subtropical western North Pacific. *Journal of Oceanography, 72*(3), 343-358. https://doi.org/10.1007/s10872-015-0346-9

Holm-Hansen, O., Lorenzen, C. J., Holmes, R. W., & Strickland, J. D. H. (1965). Fluorometric Determination of Chlorophyll. *ICES Journal of Marine Science,* 30(1), 3-15. doi:10.1093/icesjms/30.1.3

Honda, M. C. (2020). Effective Vertical Transport of Particulate Organic Carbon in the Western North Pacific Subarctic Region. *Frontiers in Earth Science,* 8(366). doi:10.3389/feart.2020.00366

Honda, M. C., Sasai, Y., Siswanto, E., Kuwano-Yoshida, A., Aiki, H., & Cronin, M. F. (2018). Impact of cyclonic eddies and typhoons on biogeochemistry in the oligotrophic ocean

based on biogeochemical/physical/meteorological time-series at station KEO. *Progress in Earth and Planetary Science, 5*(1), 42. https://doi.org/10.1186/s40645-018-0196-3

Honda, M. C., Wakita, M., Matsumoto, K., Fujiki, T., Siswanto, E., Sasaoka, K., et al. (2017). Comparison of carbon cycle between the western Pacific subarctic and subtropical time-series stations: highlights of the K2S1 project. *Journal of Oceanography, 73*(5), 647-667. https://doi.org/10.1007/s10872-017-0423-3

Hosoda, S., Ohira, T., Sato, K., & Suga, T. (2010). Improved description of global mixed-layer depth using Argo profiling floats. *Journal of Oceanography, 66*(6), 773-787. https://doi.org/10.1007/s10872-010-0063-3

Inoue, R., & Kouketsu, S. (2016). Physical oceanographic conditions around the S1 mooring site. *Journal of Oceanography, 72*(3), 453-464. https://doi.org/10.1007/s10872-015-0342-0

Irwin, A. J., Finkel, Z. V., Schofield, O. M. E., & Falkowski, P. G. (2006). Scaling-up from nutrient physiology to the size-structure of phytoplankton communities. *Journal of Plankton Research, 28*(5), 459-471. https://doi.org/10.1093/plankt/fbi148

Karl, D. M., Dore, J. E., Lukas, R., Michaels, A. F., Bates, N. R., & Knap, A. (2001). Building the Long-Term Picture: The U.S. JGOFS Time-Series Programs. *Oceanography*, 14(4), 6-17. https://doi.org/10.5670/oceanog.2001.02

Karl, D. M., & Lukas, R. (1996). The Hawaii Ocean Time-series (HOT) program: Background, rationale and field implementation. *Deep Sea Research Part II: Topical Studies in Oceanography*, 43(2), 129-156. https://doi.org/10.1016/0967-0645(96)00005-7

Kobari, T., Nakamura, R., Unno, K., Kitamura, M., Tanabe, K., Nagafuku, H., et al. (2016). Seasonal variability in carbon demand and flux by mesozooplankton communities at subarctic and subtropical sites in the western North Pacific Ocean. *Journal of Oceanography, 72*(3), 403-418. https://doi.org/10.1007/s10872-015-0348-7

Komori, N., Takahashi, K., Komine, K., Motoi, T., Zhang, X., & Sagawa, G. (2005). Description of Sea-Ice Component of Coupled Ocean–Sea-Ice Model for the Earth Simulator (OIFES). *Journal of the Earth Simulator, 4*, 31-45. https://doi.org/10.32131/jes.4.31

Kouketsu, S., Kaneko, H., Okunishi, T., Sasaoka, K., Itoh, S., Inoue, R., & Ueno, H. (2016). Mesoscale eddy effects on temporal variability of surface chlorophyll a in the Kuroshio Extension. *Journal of Oceanography, 72*(3), 439-451. https://doi.org/10.1007/s10872-015-0286-4

709 Kouketsu, S., Tomita, H., Oka, E., Hosoda, S., Kobayashi, T., & Sato, K. (2012). The role of
710 meso-scale eddies in mixed layer deepening and mode water formation in the western
711 North Pacific. *Journal of Oceanography, 68*(1), 63-77. https://doi.org/10.1007/s10872-
712 011-0049-9
713 Mahadevan, A., D'Asaro, E., Lee, C., & Perry, M. J. (2012). Eddy-Driven Stratification Initiates
714 North Atlantic Spring Phytoplankton Blooms. *Science, 337*(6090), 54-58.
715 https://doi.org/10.1126/science.1218740
716 Masumoto, Y., Sasaki, H., Kagimoto, T., Komori, N., Ishida, A., Sasai, Y., et al. (2004). A Fifty-
717 Year Eddy-Resolving Simulation of the World Ocean – Preliminary Outcomes of OFES
718 (OGCM for the Earth Simulator) –. *Journal of the Earth Simulator, 1*, 35-56.
719 https://doi.org/10.32131/jes.1.35
720 Matsumoto, K., Abe, O., Fujiki, T., Sukigara, C., & Mino, Y. (2016). Primary productivity at the
721 time-series stations in the northwestern Pacific Ocean: is the subtropical station
722 unproductive? *Journal of Oceanography, 72*(3), 359-371. https://doi.org/10.1007/s10872-
723 016-0354-4
724 Michaels, A. F., & Knap, A. H. (1996). Overview of the U.S. JGOFS Bermuda Atlantic Time-
725 series Study and the Hydrostation S program. *Deep Sea Research Part II: Topical Studies*
726 *in Oceanography, 43*(2), 157-198. https://doi.org/10.1016/0967-0645(96)00004-5
727 Morel, A., Huot, Y., Gentili, B., Werdell, P. J., Hooker, S. B., & Franz, B. A. (2007). Examining
728 the consistency of products derived from various ocean color sensors in open ocean (Case
729 1) waters in the perspective of a multi-sensor approach. *Remote Sensing of Environment*,
730 111(1), 69-88. https://doi.org/10.1016/j.rse.2007.03.012
731 Oka, E., Qiu, B., Takatani, Y., Enyo, K., Sasano, D., Kosugi, N., et al. (2015). Decadal
732 variability of Subtropical Mode Water subduction and its impact on biogeochemistry.
733 *Journal of Oceanography, 71*(4), 389-400. https://doi.org/10.1007/s10872-015-0300-x
734 Omand, M. M., D'Asaro, E. A., Lee, C. M., Perry, M. J., Briggs, N., Cetinić, I., & Mahadevan,
735 A. (2015). Eddy-driven subduction exports particulate organic carbon from the spring
736 bloom. *Science*, 348(6231), 222-225. doi:10.1126/science.1260062
737 Onogi, K., Tsutsui, J., Koide, H., Sakamoto, M., Kobayashi, S., Hatsushika, H., et al. (2007).
738 The JRA-25 Reanalysis. *Journal of the Meteorological Society of Japan. Ser. II, 85*(3),
739 369-432. https://doi.org/10.2151/jmsj.85.369

Oschlies, A. (2001). Model-derived estimates of new production: New results point towards lower values. *Deep Sea Research Part II: Topical Studies in Oceanography*, *48*(10), 2173-2197. https://doi.org/10.1016/S0967-0645(00)00184-3

Parsons, T. R., Takahashi, M., & Hargrave, B. (1984). *Biological oceanographic processes (3rd ed.)*. Oxford, U.K.: Pergamon Press.

Qiu, B., Chen, S., Klein, P., Sasaki, H., & Sasai, Y. (2014). Seasonal Mesoscale and Submesoscale Eddy Variability along the North Pacific Subtropical Countercurrent. *Journal of Physical Oceanography, 44*(12), 3079-3098. https://doi.org/10.1175/jpo-d-14-0071.1

Sasai, Y., Ishida, A., Sasaki, H., Kawahara, S., Uehara, H., & Yamanaka, Y. (2006). A Global Eddy-Resolving Coupled Physical-Biological Model: Physical Influences on a Marine Ecosystem in the North Pacific. *SIMULATION, 82*(7), 467-474. https://doi.org/10.1177/0037549706068943

Sasai, Y., Richards, K. J., Ishida, A., & Sasaki, H. (2010). Effects of cyclonic mesoscale eddies on the marine ecosystem in the Kuroshio Extension region using an eddy-resolving coupled physical-biological model. *Ocean Dynamics, 60*(3), 693-704. https://doi.org/10.1007/s10236-010-0264-8

Sasaki, H., Klein, P., Qiu, B., & Sasai, Y. (2014). Impact of oceanic-scale interactions on the seasonal modulation of ocean dynamics by the atmosphere. *Nature Communications, 5*(1), 5636. https://doi.org/10.1038/ncomms6636

Shiozaki, T., Ito, S., Takahashi, K., Saito, H., Nagata, T., & Furuya, K. (2014). Regional variability of factors controlling the onset timing and magnitude of spring algal blooms in the northwestern North Pacific. *Journal of Geophysical Research: Oceans*, 119(1), 253-265. doi:10.1002/2013JC009187

Siswanto, E., Matsumoto, K., Honda, M. C., Fujiki, T., Sasaoka, K., & Saino, T. (2015). Reappraisal of meridional differences of factors controlling phytoplankton biomass and initial increase preceding seasonal bloom in the northwestern Pacific Ocean. *Remote Sensing of Environment, 159*, 44-56. https://doi.org/10.1016/j.rse.2014.11.028

Steinberg, D. K., Carlson, C. A., Bates, N. R., Johnson, R. J., Michaels, A. F., & Knap, A. H. (2001). Overview of the US JGOFS Bermuda Atlantic Time-series Study (BATS): a decade-scale look at ocean biology and biogeochemistry. *Deep Sea Research Part II:*

Topical Studies in Oceanography, 48(8–9), 1405-1447. https://doi.org/10.1016/S0967-0645(00)00148-X

Suga, T., & Hanawa, K. (1990). The mixed-layer climatology in the northwestern part of the North Pacific subtropical gyre and the formation area of Subtropical Mode Water. *Journal of Marine Research, 48*(3), 543-566. https://doi.org/10.1357/002224090784984669

Suga, T., Hanawa, K., & Toba, Y. (1989). Subtropical Mode Water in the 137°E Section. *Journal of Physical Oceanography, 19*(10), 1605-1618. https://doi.org/10.1175/1520-0485(1989)019<1605:smwits>2.0.co;2

Sugimoto, S., & Hanawa, K. (2010). Impact of Aleutian Low activity on the STMW formation in the Kuroshio recirculation gyre region. *Geophysical Research Letters, 37*(3). https://doi.org/10.1029/2009gl041795

Sugimoto, S., & Kako, S. i. (2016). Decadal Variation in Winter Mixed Layer Depth South of the Kuroshio Extension and Its Influence on Winter Mixed Layer Temperature. *Journal of Climate, 29*(3), 1237-1252. https://doi.org/10.1175/jcli-d-15-0206.1

Sukigara, C., Suga, T., Saino, T., Toyama, K., Yanagimoto, D., Hanawa, K., & Shikama, N. (2011). Biogeochemical evidence of large diapycnal diffusivity associated with the subtropical mode water of the North Pacific. *Journal of Oceanography, 67*(1), 77-85. https://doi.org/10.1007/s10872-011-0008-5

Suzuki, R., & Ishimaru, T. (1990). An Improved Method for the Determination of Phytoplankton Chlorophyll using N, N-Dimethlformamide. *Journal of the Oceanographical Society of Japan*, 46(4), 190-194. doi:10.1007/BF02125580

Sverdrup, H. U. (1953). On Conditions for the Vernal Blooming of Phytoplankton. *ICES Journal of Marine Science*, 18(3), 287-295. https://doi.org/10.1093/icesjms/18.3.287

Taylor, J. R., & Ferrari, R. (2011). Shutdown of turbulent convection as a new criterion for the onset of spring phytoplankton blooms. *Limnology and Oceanography, 56*(6), 2293-2307. https://doi.org/10.4319/lo.2011.56.6.2293

Ueda, H., Amagai, Y., & Hayasaki, M. (2017). South-coast cyclone in Japan during El Niño-caused warm winters. *Asia-Pacific Journal of Atmospheric Sciences, 53*(2), 287-293. https://doi.org/10.1007/s13143-017-0025-4

Uehara, H., Suga, T., Hanawa, K., & Shikama, N. (2003). A role of eddies in formation and transport of North Pacific Subtropical Mode Water. *Geophysical Research Letters, 30*(13). https://doi.org/10.1029/2003gl017542

Wakita, M., Honda, M. C., Matsumoto, K., Fujiki, T., Kawakami, H., Yasunaka, S., et al. (2016). Biological organic carbon export estimated from the annual carbon budget observed in the surface waters of the western subarctic and subtropical North Pacific Ocean from 2004 to 2013. *Journal of Oceanography, 72*(5), 665-685. https://doi.org/10.1007/s10872-016-0379-8

Zarubin, M., Lindemann, Y., & Genin, A. (2017). The dispersion-confinement mechanism: Phytoplankton dynamics and the spring bloom in a deeply-mixing subtropical sea. *Progress in Oceanography, 155*, 13-27. https://doi.org/10.1016/j.pocean.2017.05.005

812 **Figure captions**

813 **Figure 1.** Location of station S1 (30°N, 145°E) with (a) prevailing surface currents, and (b)
814 monthly averaged mixed-layer depth based on a 0.125 kg m^{-3} criterion determined from the
815 MIxed Layer dataset of Argo, Grid Point Value between January and April.
816
817 **Figure 2.** Seasonal variations of (a) photosynthetically active radiation (PAR), (b) temperature,
818 (c) nitrate concentrations, and (d) chl-*a* concentrations at the sea surface. Satellite data are shown
819 by daily (black plus symbols) and monthly (orange circles; error bars indicate standard
820 deviations) spatial averages across a 100 km × 100 km box centered at S1. Averages were
821 calculated from MODIS satellite data with a 4-km spatial resolution. Shipboard measurements
822 (blue crosses) conducted in 2010 and 2011 have been merged by year and sorted in order of
823 season. The chl-*a* data focus on bloom seasons in 2010 and 2011, and spatial means (black plus
824 symbols) and maxima (red plus symbols) in the box are also shown in (d'). The dashed line
825 indicates the bloom threshold, which was 0.4 mg m^{-3} chl-*a*.
826
827 **Figure 3.** Satellite images of chl-*a* and sea-surface temperature (SST) around S1 (2° × 2° grid)
828 with a 1-km spatial resolution during the winter (22 Feburuary) and early spring (2 and 6 April)
829 of 2010 and the winter (25 Feburuary) and late spring (14 and 21 April) of 2011. The black color
830 show pixels with no data. The relationships between chl-*a* and SST are plotted to the right of the
831 satellite images, and chl-*a* peaks are denoted by arrows. The dashed lines in the right panels
832 indicate the bloom threshold of 0.4 mg m^{-3} chl-*a*.
833
834 **Figure 4.** Seasonal variations in water column stability from January to May in 2010 and 2011.
835 The upper panels show two measures of mixed-layer depth (MLD), $MLD_{0.03\sigma\theta}$ (red bars; based
836 on a 0.03 kg m^{-3} criterion) and $MLD_{0.125\sigma\theta}$ (black bars; based on a 0.125 kg m^{-3} criterion), and
837 monthly-averaged critical depth (green lines). MLDs were calculated from 10-d averages of the
838 MIxed Layer dataset of Argo, Grid Point Value (MILA GPV). In-situ MLDs acquired five
839 typical vertical profiles in the lower panels and other in-situ MLDs through the shipboard
840 observations are also indicated by different symbols. The lower panels show five typical vertical
841 profiles of temperature (black lines), nitrate (blue circles), chl-*a* (red circles), and MLDs
842 ($MLD_{0.03\sigma\theta}$: dotted lines; $MLD_{0.125\sigma\theta}$: solid lines) acquired from shipboard observations on the

basis of water column stability during winter and spring. Dashed lines indicate the bloom threshold of 0.4 mg m^{-3} chl-*a*. Measurements were made by shipboard observation on the following dates: A, 31 Jan 2010; B, 9 Feb. 2010; C, 14 Feb. 2011; D, 30 Apr. 2011; and E, 28 Apr. 2011. Details are provided in the text.

Figure 5. Conceptual illustration of subtropical bloom formation in (1) winter, (2) early spring, and (3) late spring based on water column stability. Subtropical blooms are shown as yellow circles. Values of MLDs from MIxed Layer dataset of Argo, Grid Point Value (MILA GPV) data ($MLD_{0.03\sigma\theta}$: red line; $MLD_{0.125\sigma\theta}$: black line), and critical depth (green line) were determined based on climatological data. Episodic stratification after the development of winter mixing and the breakdown of stratification is indicated by red dotted lines.

Figure 6. Two measures of mixed-layer depth, $MLD_{0.03\sigma\theta}$ (red lines; based on a 0.03 kg m^{-3} criterion) and $MLD_{0.125\sigma\theta}$ (black lines; based on a 0.125 kg m^{-3} criterion), were determined from MIxed Layer dataset of Argo, Grid Point Value (MILA GPV) data. Two time periods (2002–2003 and 2010–2011) are indicated by shading.

Figure 7. Seasonal variations from January to May of 2002 and 2003 of modeled nitrate (upper panels) and phytoplankton biomass (middle panels) (shown in nitrogen concentration units), and satellite-observed sea-surface chl-*a* concentrations (lower panels). Sea-surface chl-*a* was obtained from SeaWiFS data in 2002 and MODIS in 2003. Values were calculated as spatial means (black plus symbols) and maxima (red plus symbols) within a 100 km × 100 km box centered at S1 with 9-km (SeaWiFs) and 4-km (MODIS) spatial resolution. White lines in the upper panels denote a nitrate concentration of 0.1 μM. White lines and red lines in the middle panels denote $MLD_{0.03\sigma\theta}$ and $MLD_{0.125\sigma\theta}$, respectively. MLDs determined by MIxed Layer dataset of Argo, Grid Point Value (MILA GPV) data ($MLD_{0.03\sigma\theta}$: dotted yellow bars; $MLD_{0.125\sigma\theta}$: solid yellow bars) are superimposed on the middle panels. The dashed lines in the bottom panels indicate the bloom threshold of 0.4 mg m^{-3} chl-*a*. Time periods corresponding to the typical vertical profiles shown in Figure 4 are noted at the top of the figure.

Figure 1.

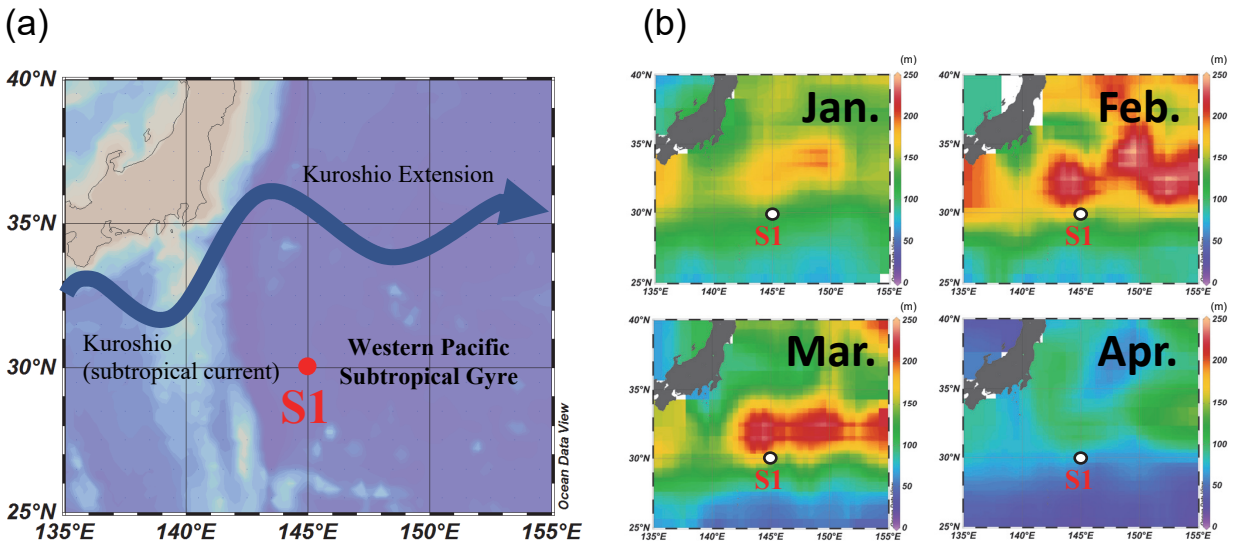
(a)
(b)
40°N
35°N
30°N
25°N
135°E
140°E
145°E
150°E
155°E
Kuroshio Extension
Kuroshio
(subtropical current)
Western Pacific
Subtropical Gyre
S1
Ocean Data View
Jan.
Feb.
Mar.
Apr.
(m)
250
200
150
100
50
0

Figure 2.

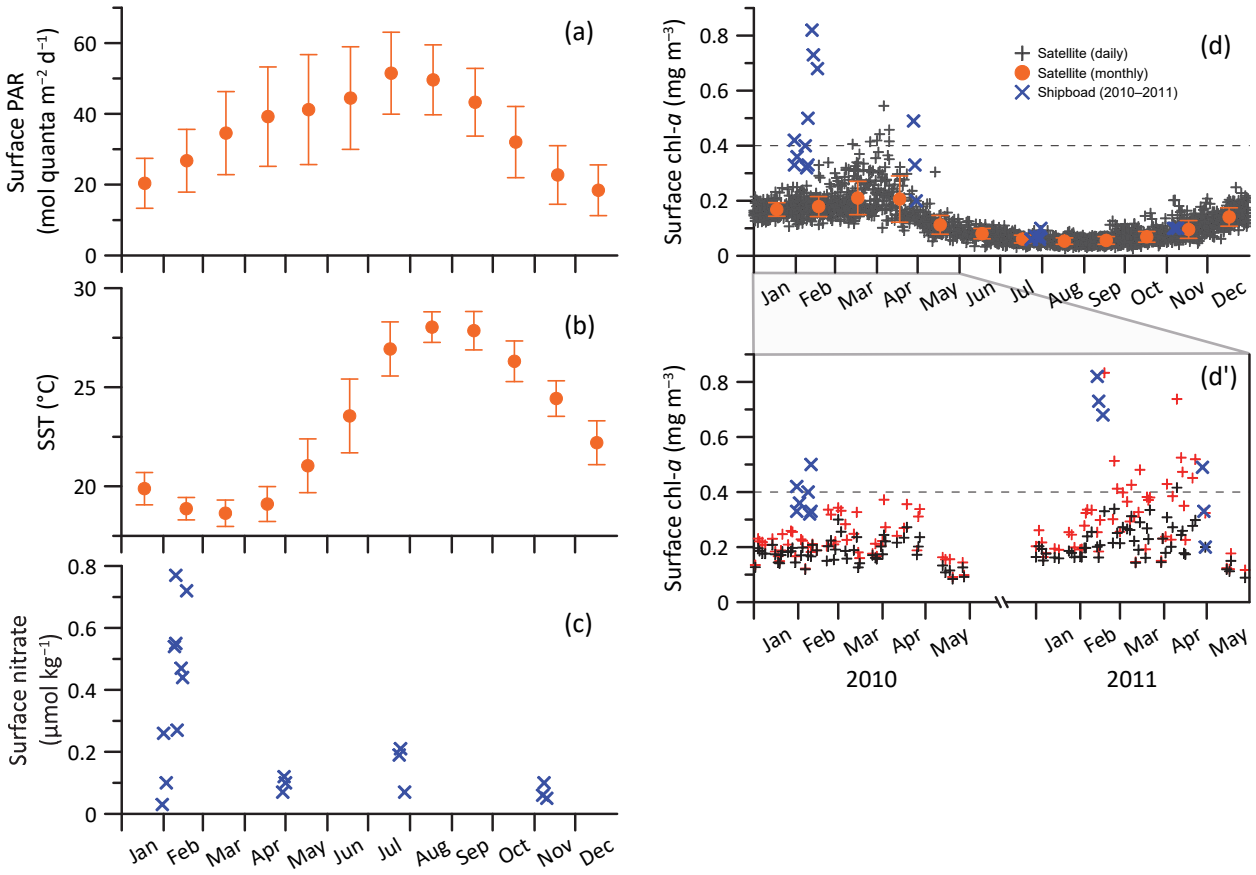
(a)
Surface PAR
(mol quanta m^{-2} d^{-1})
0
20
40
60
(b)
SST (°C)
20
25
30
(c)
Surface nitrate
(µmol kg^{-1})
0
0.2
0.4
0.6
0.8
Jan Feb Mar Apr May Jun Jul Aug Sep Oct Nov Dec
(d)
Satellite (daily)
Satellite (monthly)
Shipboad (2010–2011)
Surface chl-a (mg m^{-3})
0
0.2
0.4
0.6
0.8
Jan Feb Mar Apr May Jun Jul Aug Sep Oct Nov Dec
(d')
Surface chl-a (mg m^{-3})
0
0.2
0.4
0.6
0.8
Jan Feb Mar Apr May
2010
Jan Feb Mar Apr May
2011

Figure 3.

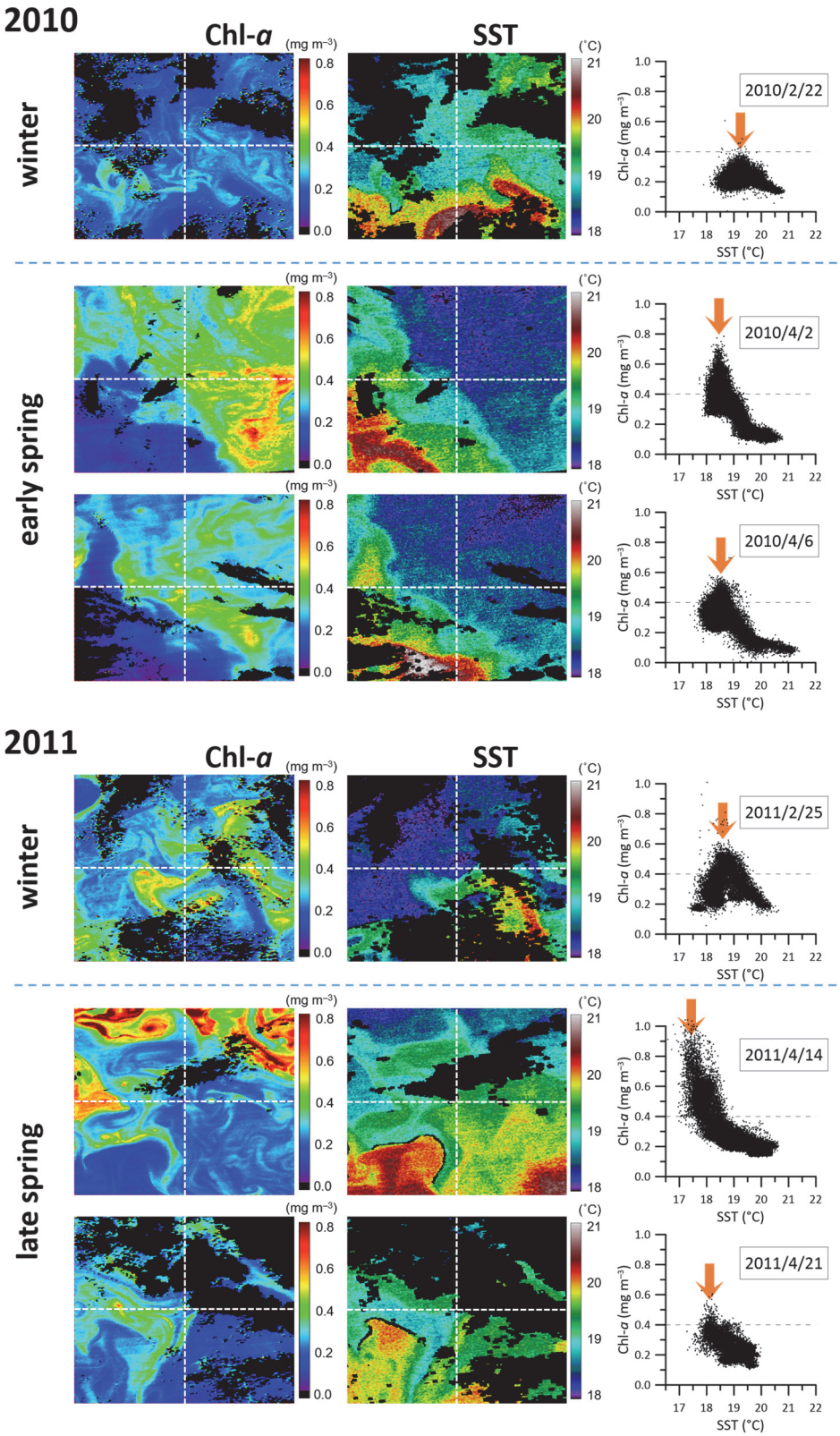
2010
Chl-a
SST
winter
early spring
2011
winter
late spring
(mg m⁻³)
(°C)
0.0
0.2
0.4
0.6
0.8
18
19
20
21
17
18
19
20
21
22
Chl-a (mg m⁻³)
SST (°C)
2010/2/22
2010/4/2
2010/4/6
2011/2/25
2011/4/14
2011/4/21

Figure 4.

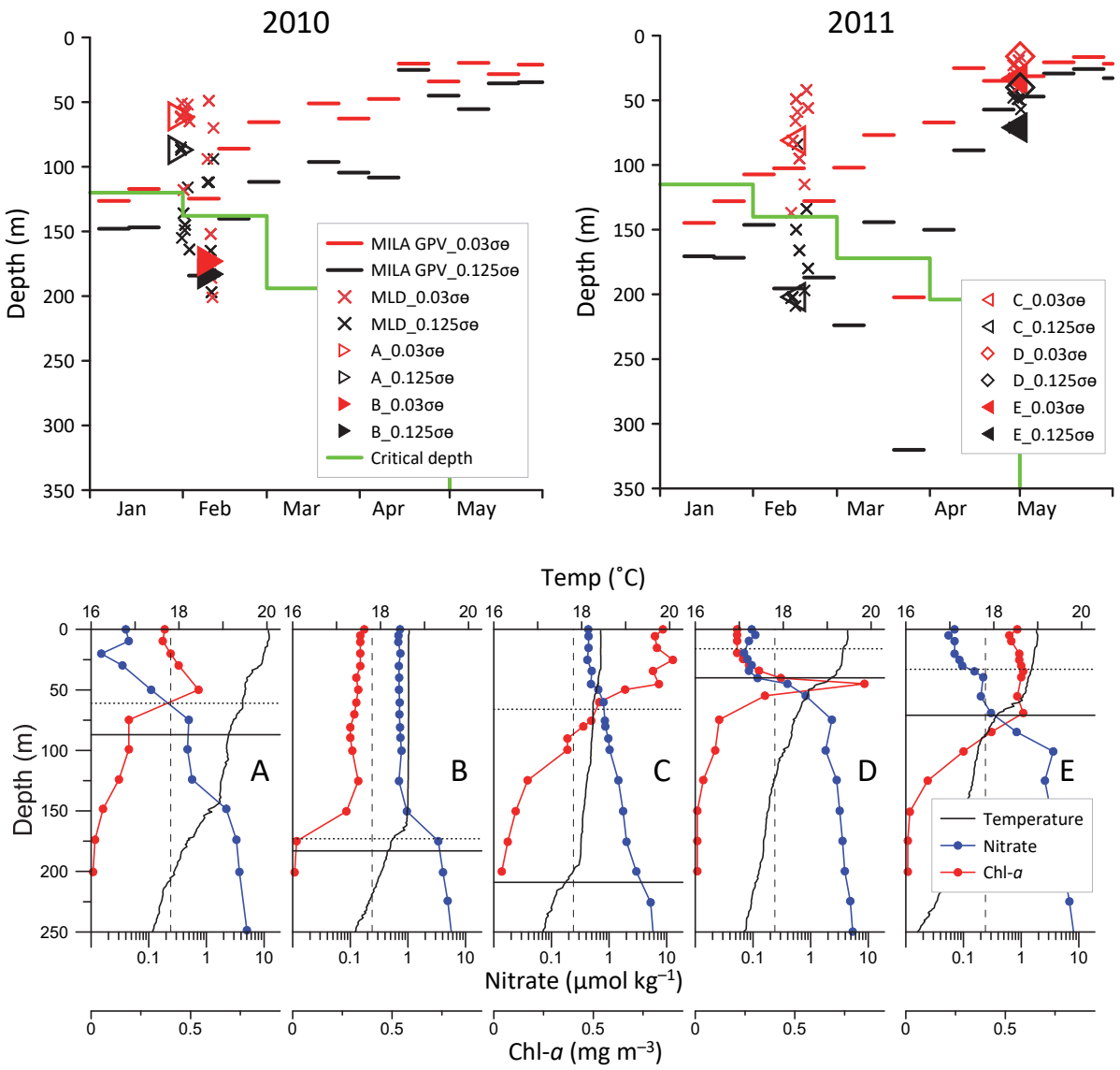
2010
2011
Depth (m)
0
50
100
150
200
250
300
350
Jan
Feb
Mar
Apr
May
MILA GPV_0.03σθ
MILA GPV_0.125σθ
MLD_0.03σθ
MLD_0.125σθ
A_0.03σθ
A_0.125σθ
B_0.03σθ
B_0.125σθ
Critical depth
C_0.03σθ
C_0.125σθ
D_0.03σθ
D_0.125σθ
E_0.03σθ
E_0.125σθ
Temp (˚C)
16
18
20
A
B
C
D
E
Temperature
Nitrate
Chl-a
0.1
1
10
Nitrate (µmol kg⁻¹)
0
0.5
Chl-a (mg m⁻³)

Figure 5.

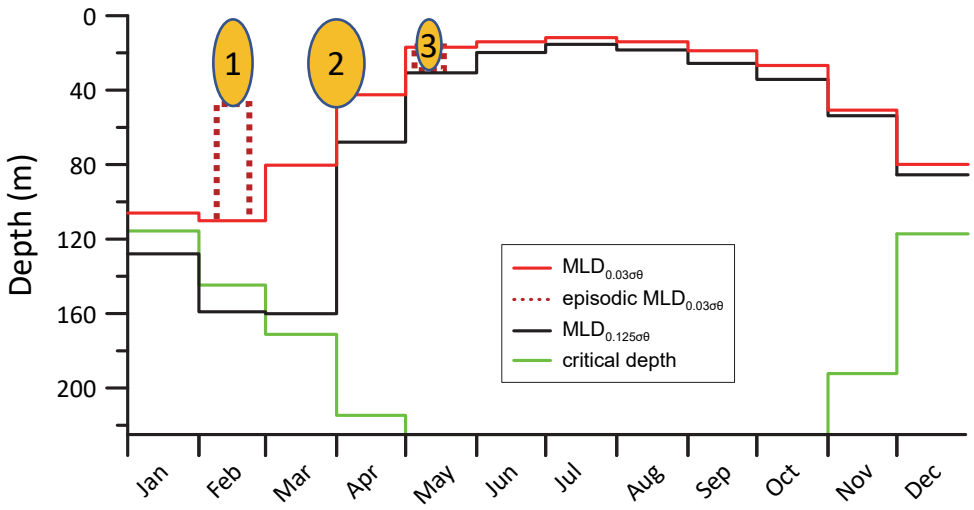
Depth (m)
0
40
80
120
160
200
1
2
3
Jan
Feb
Mar
Apr
May
Jun
Jul
Aug
Sep
Oct
Nov
Dec
MLD0.03σθ
episodic MLD0.03σθ
MLD0.125σθ
critical depth

Figure 6.

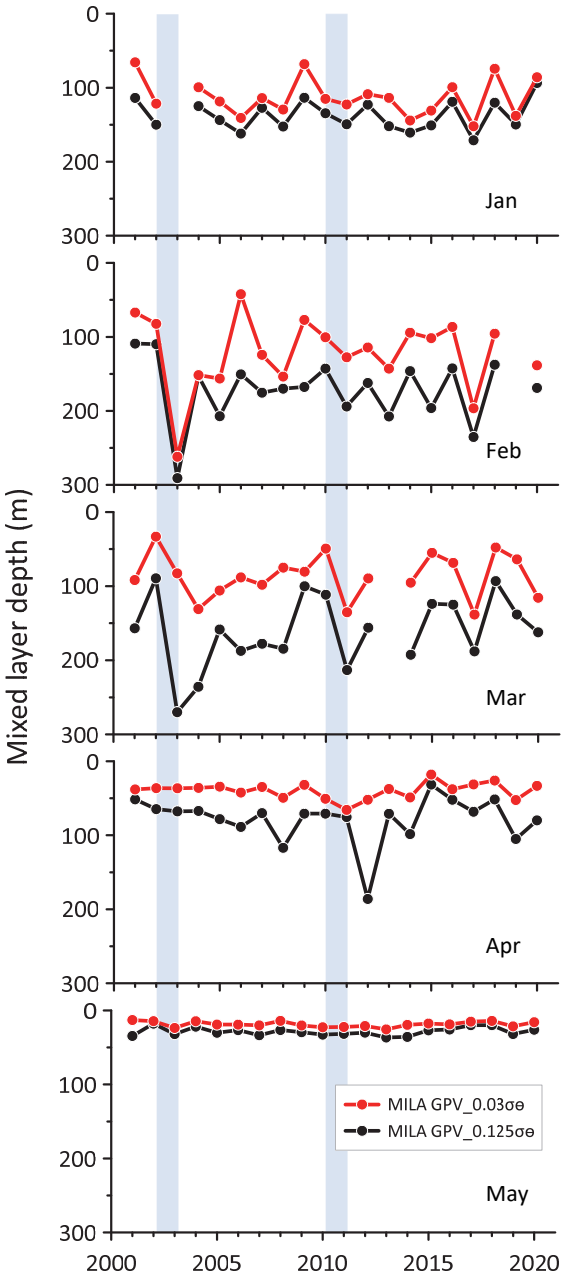
Mixed layer depth (m)
0
100
200
300
Jan
Feb
Mar
Apr
May
2000
2005
2010
2015
2020
MILA GPV_0.03σθ
MILA GPV_0.125σθ

Figure 7.

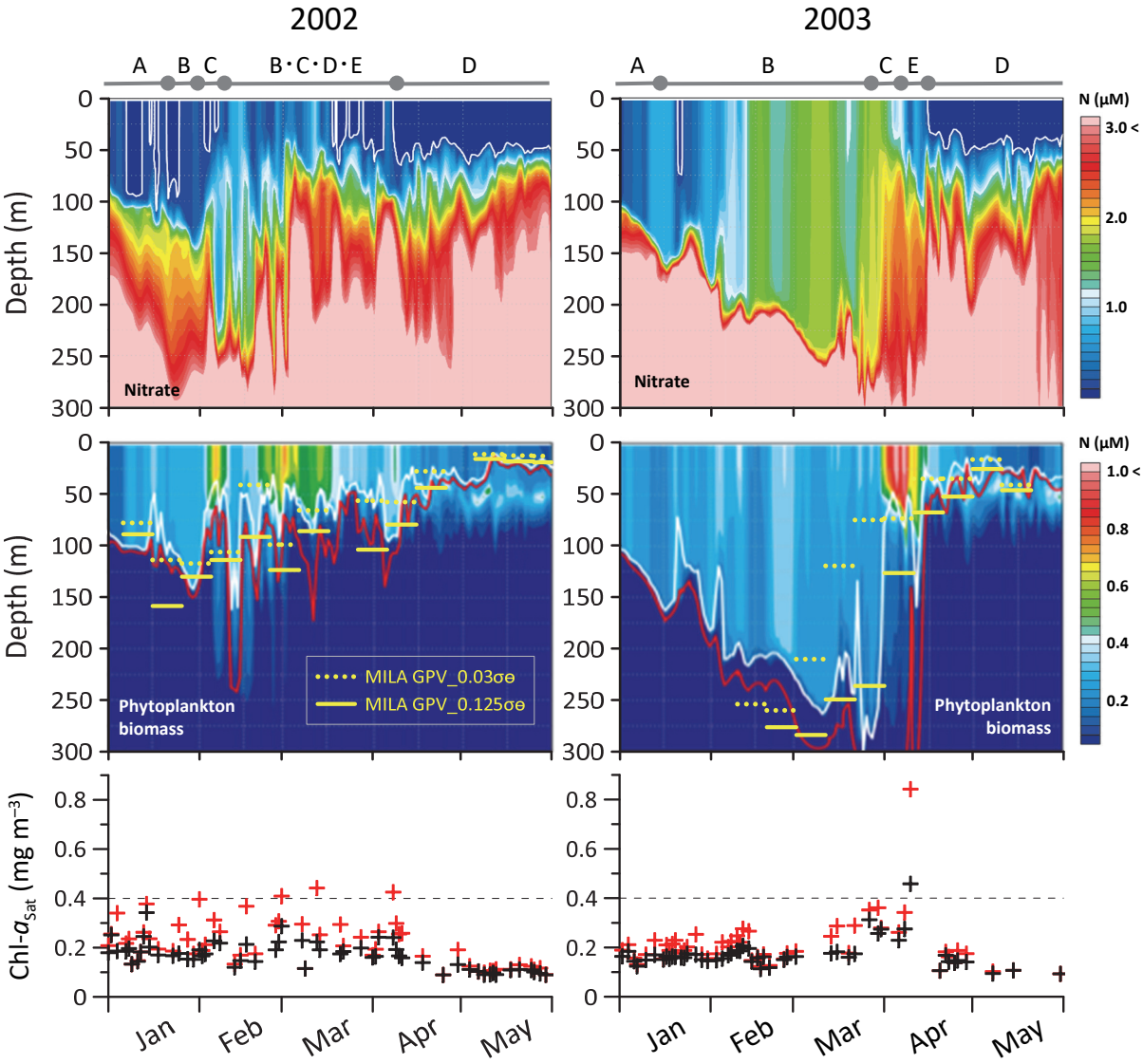
2002
2003
A
B
C
B·C·D·E
D
A
B
C
E
D
Depth (m)
Nitrate
N (μM)
3.0 <
2.0
1.0
Phytoplankton biomass
MILA GPV_0.03σθ
MILA GPV_0.125σθ
1.0 <
0.8
0.6
0.4
0.2
Chl-a_{sat} (mg m^{-3})
Jan
Feb
Mar
Apr
May